Mass Footprints of the North Pacific Atmospheric Blocking Highs

TAE-WON PARK

School of Earth and Atmospheric Sciences, Georgia Institute of Technology, Atlanta, Georgia, and Department of Earth Science Education, Chonnam National University, Gwangju, South Korea

YI DENG

School of Earth and Atmospheric Sciences, Georgia Institute of Technology, Atlanta, Georgia

WENHONG LI

Earth and Ocean Sciences, Nicholas School, Duke University, Durham, North Carolina

SONG YANG

School of Environmental Science and Engineering, Sun Yat-Sen University, Guangzhou, China

MING CAI

Department of Earth, Ocean, and Atmospheric Science, Florida State University, Tallahassee, Florida

(Manuscript received 27 August 2014, in final form 15 January 2015)

ABSTRACT

The mass footprints associated with atmospheric blocks over the North Pacific are evaluated by constructing daily tendencies of total mass over the blocking domain from three-dimensional mass fluxes throughout the life cycle of a composite blocking event. The results highlight the major role of mass convergence driven by low-frequency (with periods >1 week) atmospheric disturbances during both the development and decay stage of a block. Specifically, low-frequency eddies are responsible for the accelerated mass buildup 4 days prior to the peak intensity of a block, and they also account for the rapid mass loss afterward. High-frequency, subweekly scale disturbances have statistically significant positive contributions to the mass loss during the decay stage, and also show weak negative contributions to the development of the blocking high prior to the peak of the high. The majority of the mass convergence (divergence) responsible for the intensification (decay) of the blocking high occurs in the middle-to-lower troposphere and is largely attributed to mass flux driven by low-frequency meridional (zonal) winds. Also discussed are the implications of this new mass perspective of atmospheric blocks for understanding dynamics of blocking highs and for model bias detection and attribution.

1. Introduction

Blocking highs constitute a crucial component of the extratropical atmospheric low-frequency variability. The flow fields of these ''atmospheric blocks'' are characterized by persistent anticyclones that tend to obstruct the normal zonal flow (Berggren et al. 1949; Rex 1950). Being vertically coherent and quasi-stationary, blocking highs exert strong impacts not only on local weather patterns but also on continental-scale atmospheric circulation (e.g., over the North Pacific and Euro–Atlantic regions; Carrera et al. 2004; Trigo et al. 2004).

On one hand, high-frequency (subweekly scale) transient eddies have been known to play a critical role in the development of atmospheric blocks. For example, Green (1977) suggested the importance of storm-track eddies in maintaining blocking flows. Nakamura and Wallace (1993) provided further evidence of elevated activity of high-frequency baroclinic eddies prior to the

Corresponding author address: Tae-Won Park, Department of Earth Science Education, Chonnam National University, 77 Yongbong-ro, Buk-gu, Gwangju 500-757, South Korea.
E-mail: park2760@jnu.ac.kr

DOI: 10.1175/JCLI-D-14-00598.1

onset of blocking events. Blocking formation in some general circulation models (GCMs) was also shown to be tied to dynamical forcing of high-frequency eddies (Maeda et al. 2000; Shutts 1983). On the other hand, effects of low-frequency (10–30-day period) eddies themselves are also felt throughout the life cycles of atmospheric blocks. For example, the occurrence of a quasi-stationary wave train may induce the formation of a persistent anticyclonic flow anomaly (Stewart 1993). Colucci (1985) showed that the planetary wave environment created by a vorticity source during explosive cyclogenesis can result in subsequent downstream blocking. Breaking of low-frequency Rossby waves entails reversals of the meridional gradients of potential temperature at the dynamical tropopause, which are also recognized as key features of atmospheric blocks (Pelly and Hoskins 2003). Nakamura et al. (1997) pointed out that forcing from high-frequency eddies is indispensable for blocking formation over the North Pacific, while low-frequency dynamics represented by the emergence of a quasi-stationary Rossby wave train over the North Atlantic is more important for blocking development over Europe.

From the point of view of mass change, the formation of a blocking high can be regarded as the process of mass convergence into the air column underneath which the surface high emerges. In the literature, however, no study has examined the development and decay of blocking highs from the perspective of mass accumulation and dissipation. Homeyer and Bowman (2013) investigated the mass transport between tropical and extratropical regions associated with events of Rossby wave breaking through Lagrangian trajectory calculations, but ''area transport'' instead of actual mass was dealt with in the analysis. Furthermore, the traditional diagnosis of blocking formation and dissipation tend to focus on geopotential height or vorticity tendency at specific isobaric levels and the eddy effect is quantified in terms of vorticity (momentum) flux convergence/divergence. Most quantities (e.g., eddy momentum flux) computed are in the ''per unit mass'' sense, and the actual mass weighting is not clear from the corresponding plots. A view of the blocking dynamics from the mass perspective compliments the traditional approach by providing explicit information on mass weighting. It helps to quantify the relative importance of atmospheric processes at different altitudes and along different directions (zonal versus meridional) in determining the evolution of a blocking event.

The goal of this study is to provide a preliminary, mass-circulation-based assessment of the relative roles of atmospheric eddies (motions) of different temporal scales in determining the life cycle of atmospheric blocks observed over the North Pacific. The calculations will be done in a semi-Lagrangian framework and focus on assessing the column mass divergence/convergence based upon daily three-dimensional (3D) mass flux in isentropic coordinates. Individual air parcels conserve their potential temperatures and remain on their original isentropic surfaces in the absence of diabatic heating and frictional effects (Crum and Stevens 1988). The use of isentropic coordinates thus allows us to provide accurate estimates of the 3D mass flux and the associated mass divergence and convergence.

2. Methods

The study period considered here is 1979–2010. The data used in the analysis are obtained from the European Centre for Medium-Range Weather Forecasts (ECMWF) Interim Re-Analysis (ERA-Interim) (Dee et al. 2011). Specifically, daily potential temperature (θ) on the 2-PVU surface (1 PVU = $10^{-6}\,\mathrm{K\,kg^{-1}\,m^2\,s^{-1}}$) is used to identify prominent blocking events. Mass fluxes across boundaries of blocking events are derived from daily geopotential height (Z), temperature (T), zonal and meridional winds (u and v), and vertical velocity (ω) on 36 isentropic levels, which are interpolated from 37 isobaric levels in the original ERA-Interim data.

The detection of blocking events follows the methodology of Pelly and Hoskins (2003). In this approach, the central blocking latitude ϕ_c for each longitude is first defined as the location of meridional maxima of the climatological annual mean transient eddy kinetic energy (TEKE) at 300 hPa, which is derived from the 3–7-day bandpass-filtered winds. Next, θ values on 2 PVU are averaged over two boxes of dimensions 5° longitude by 15° latitude poleward and equatorward of ϕ_c for each longitude and their difference (poleward box minus equatorward box) is calculated. These calculations are repeated at latitudes of $\phi_c - 4°$, ϕ_c, and $\phi_c + 4°$. The blocking index for each longitude is taken as the maximum of these three values. An instantaneous blocking is detected if the blocking index is positive. To identify prominent, long-lasting blocking events, we adopt the criteria that the instantaneous blocking (positive block index values) should occur over at least 10° of longitude and last at least 4 consecutive days. For the detected long-lasting blocking events, we define day 0 as the day of the first detection (i.e., when the blocking index starts to meet the above criteria). Focusing on a region extending from the eastern North Pacific to the west coast of North America (180°–120°W), we are able to detect a total of 30 major blocking events for the study period and these events are used in the subsequent composite analysis.

The calculation of mass flux is done for cuboids bounded by two adjacent isentropic levels (10 K apart, from 235 to 875 K) in the vertical and with 40° longitude and 20° latitude in the horizontal. For each blocking event, the center of the cuboid is placed at the location of the daily maximum geopotential anomaly at 300 hPa on each day when the geopotential anomaly is identifiable. In other words, event-specific, time-dependent blocking domains are used to ensure the blocking center adequately covered. The composite results are reported for the period from day −4 to day +7, which covers the essential life cycle characteristics of an atmospheric block (Croci-Maspoli et al. 2007). In an isentropic layer bounded by two adjacent isentropic levels, atmospheric mass per unit area (units of kilogram per square meter) is computed following

$$M_\theta = -\frac{1}{g}\Delta p, \tag{1}$$

where g is the gravity constant (9.81 m s^{-2}) and Δp is the pressure difference between the two levels. The mass continuity equation in isentropic coordinates used in our analysis follows Moore (1989) and can be written as

$$\frac{\partial M_\theta}{\partial t} = -\frac{1}{a\cos\phi}\frac{\partial (M_\theta u)}{\partial \lambda} - \frac{1}{a\cos\phi}\frac{\partial (M_\theta v\cos\phi)}{\partial \phi} - \frac{\partial (M_\theta \dot{\theta})}{\partial \theta}, \tag{2}$$

where the local mass tendency is expressed as the sum of the 3D mass convergence. The variables u, v, and $\dot{\theta}$ are the zonal wind, meridional wind, and vertical velocity in isentropic coordinates (i.e., the total diabatic heating rate), respectively. Here a is the mean radius of the earth. The variables λ and ϕ are the longitude and latitude, respectively. Here $\dot{\theta}$ is estimated through the thermodynamic energy equation following

$$\dot{\theta} = \frac{1}{c_p}\left(\frac{p_s}{p}\right)^{R/c_p}\left[c_p\left(\frac{\partial T}{\partial t} + \frac{u}{a\cos\phi}\frac{\partial T}{\partial \lambda} + \frac{v}{a}\frac{\partial T}{\partial \phi} + \omega\frac{\partial T}{\partial p}\right) - \frac{RT}{p}\omega\right], \tag{3}$$

where c_p is the specific heat at constant pressure (=1004 J kg^{-1} K^{-1}), p is pressure, p_s is a reference pressure (usually taken to be 1000 hPa), T is the temperature, ω is the pressure vertical velocity (obtained from the ERA-Interim), and R is gas constant for dry air (=287 J K^{-1} kg^{-1}).

Applying Eq. (2) to the North Pacific blocking, the local mass change within blocking domain can be estimated as the vertical sum (over all cuboids) of the net convergence of mass into each cuboid bounded by two adjacent isentropic levels. The net convergence of mass into each cuboid itself is the sum of three components: the convergence in the zonal, meridional, and vertical direction. Zonal mass convergence can be estimated as the difference of the zonal mass fluxes (mfx) between the western and eastern boundary of the cuboid. Zonal mass flux at the western or eastern boundary is calculated by multiplying the local mass per unit area (M_θ) by the meridional length of the data grid box and zonal wind, and the zonal mass convergence is thus

$$\begin{aligned}\mathrm{mc}_{\mathrm{zonal}} &= \sum_{\mathrm{wb}} \mathrm{mfx} - \sum_{\mathrm{eb}} \mathrm{mfx} \\ &= \sum_{\mathrm{wb}} M_{\theta \mathrm{wb}} a\Delta\phi u_{\mathrm{wb}} - \sum_{\mathrm{eb}} M_{\theta \mathrm{eb}} a\Delta\phi u_{\mathrm{eb}},\end{aligned} \tag{4}$$

where wb and eb stand for western boundary and eastern boundary, respectively; $\Delta\phi$ is the latitude interval (1.5°); and Σ indicates summation over all grid boxes along the western or eastern boundary of the cuboid. In a similar manner, meridional mass convergence can be written as

$$\begin{aligned}\mathrm{mc}_{\mathrm{meridional}} &= \sum_{\mathrm{sb}} \mathrm{mfy} - \sum_{\mathrm{nb}} \mathrm{mfy} = \sum_{\mathrm{sb}} M_{\theta \mathrm{sb}} a\cos\phi\Delta\lambda v_{\mathrm{sb}} \\ &\quad - \sum_{\mathrm{nb}} M_{\theta \mathrm{nb}} a\cos\phi\Delta\lambda v_{\mathrm{nb}},\end{aligned} \tag{5}$$

Where sb and nb stand for southern boundary and northern boundary, respectively; $\Delta\lambda$ is the longitude interval (1.5°); and Σ indicates summation over all grid boxes along the southern or northern boundary of the cuboid. Vertical mass convergence into a cuboid is calculated as the difference between mass flux escaping through the upper level and mass flux coming into through the lower level. Mass flux in the vertical direction is a product of the "density" (in the units of per unit area per kelvin), isentropic vertical velocity, and the horizontal area of the data grid box. The area of the horizontal grid box (A) is estimated by considering it an isosceles trapezoid with the height $a\Delta\phi$, the top length $a\cos(\phi + 0.5\phi)\Delta\lambda$, and the base length $a\cos(\phi - 0.5\phi)\Delta\lambda$. Thus, the vertical mass convergence is written as

$$\begin{aligned}\mathrm{mc}_{\mathrm{vertical}} &= \sum_{\mathrm{lb}} \mathrm{mf}\theta - \sum_{\mathrm{ub}} \mathrm{mf}\theta \\ &= \sum_{\mathrm{lb}} M_{\theta \mathrm{lb}} A\frac{\dot{\theta}_{\mathrm{lb}}}{\Delta\theta_{\mathrm{lb}}} - \sum_{\mathrm{ub}} M_{\theta \mathrm{ub}} A\frac{\dot{\theta}_{\mathrm{ub}}}{\Delta\theta_{\mathrm{ub}}},\end{aligned} \tag{6}$$

where lb and ub stand for lower boundary and upper boundary, respectively. Note that division by $\Delta\theta$ in Eq. (6) gives the density. The Σ indicates summation over all

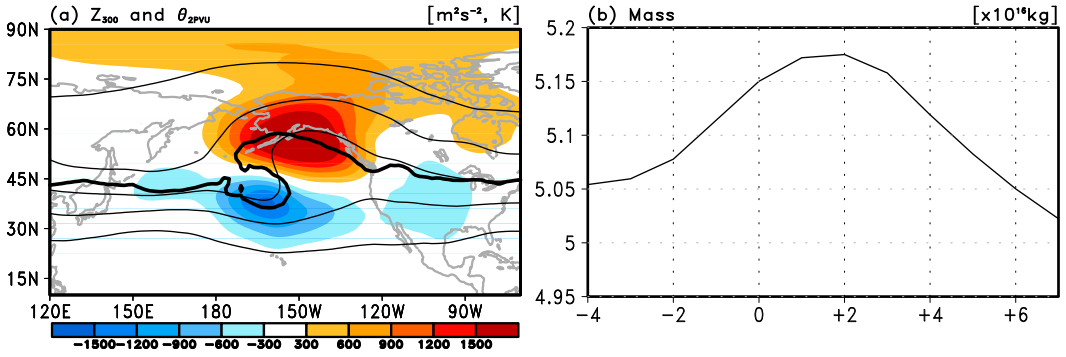

FIG. 1. (a) The composite geopotential at 300 hPa (contour with an interval of 20 $m^2 s^{-2}$) and the corresponding anomaly (shading; $m^2 s^{-2}$) for the North Pacific blocking. The thick black solid line indicates the θ contour of 326 K on the surface where PVU = 2. (b) Temporal evolution of the total mass (kg) within the blocking domain above 280 K.

grid boxes in the horizontal surface at the lower or upper boundary. Note that mass flux across vertical (lower and upper) boundaries is derived from isentropic vertical velocity (i.e., the diabatic heating rate). Thus, the 3D mass flux analysis can consider the diabatic effects in blocking dynamics. Averaged over a predefined horizontal domain, the vertical structure of vertical mass flux captured by this analysis can reveal the influence of diabatic heating at different altitudes in contributing to the vertical mass redistribution during the life cycle of atmospheric blocking.

To investigate the contributions of atmospheric eddies of different time scales to the total mass flux convergence, we further decompose the mass flux across the horizontal and vertical boundaries of a cuboid into those associated with mass and wind fluctuations at high and low frequencies. Specifically, we separate the total mass (in terms of M_θ) and the total winds into a high-frequency component (obtained via 6-day high-pass filter) and a low-frequency/stationary component (obtained as the difference between the total and high-pass filtered value) following

$$M_\theta \mathbf{V} = (M_{\theta\text{high}} + M_{\theta\text{low}})(\mathbf{V}_{\text{high}} + \mathbf{V}_{\text{low}}) = \underbrace{M_{\theta\text{high}}\mathbf{V}_{\text{high}}}_{\text{(i)}} + \underbrace{M_{\theta\text{low}}\mathbf{V}_{\text{low}}}_{\text{(ii)}} + \underbrace{M_{\theta\text{high}}\mathbf{V}_{\text{low}} + M_{\theta\text{low}}\mathbf{V}_{\text{high}}}_{\text{(iii)}}, \tag{7}$$

where $\mathbf{V} = (u, v, \dot{\theta})$ is the 3D wind vector in isentropic coordinates. According to Eq. (7), this decomposition produces three parts in the mass flux: (i) flux due to high-frequency eddies, (ii) flux due to low-frequency/stationary eddies, and (iii) flux due to the interaction between high- and low-frequency/stationary eddies.

3. Results

Figure 1a shows the composite mean 300-hPa geopotential (contours) and the corresponding anomaly field (shading) for the identified 30 North Pacific blocking events on day 0. The positive geopotential anomaly characterizing the blocking sits over southern Alaska with local maximum values reaching 1500 $m^2 s^{-2}$. A weaker negative geopotential anomaly is found southwest of the blocking high. Intrusion of a high-θ (high potential temperature) air mass into the high latitudes is clearly visible through the folding of the 326-K θ contour (thick solid line in Fig. 1a). The poleward extrusion of high-θ air is more pronounced compared to the equatorward extrusion of low-θ air. The overturning occurs primarily cyclonically and thus the composite blocking represents dynamically a warm-cyclonic Rossby wave breaking event (Masato et al. 2012). Figure 1b plots the temporal evolution of the air mass above 280-K θ surface over the blocking area (±20° longitude and ±10° latitude from the center of the blocking defined as the location of the maximum daily 300-hPa geopotential anomaly) throughout the composited life cycle of blocking events (from day −4 to day +7). Note that the 280-K surface is used here instead of the actual surface to avoid the relatively large errors produced when near-surface data are interpolated from isobaric to isentropic levels (Ziv and Alpert 1994). Furthermore, the air mass above 280 K on average accounts for 97% of the total mass in a column, and this allows our calculations to capture the majority of the processes responsible for the mass accumulation and dissipation during the life cycle of the blocking events. Figure 1b shows that the mass in the blocking domain steadily increases starting from day −4 and the increase accelerates on day −2. The mass reaches its peak value around day +2, approximately 2 days after the blocking

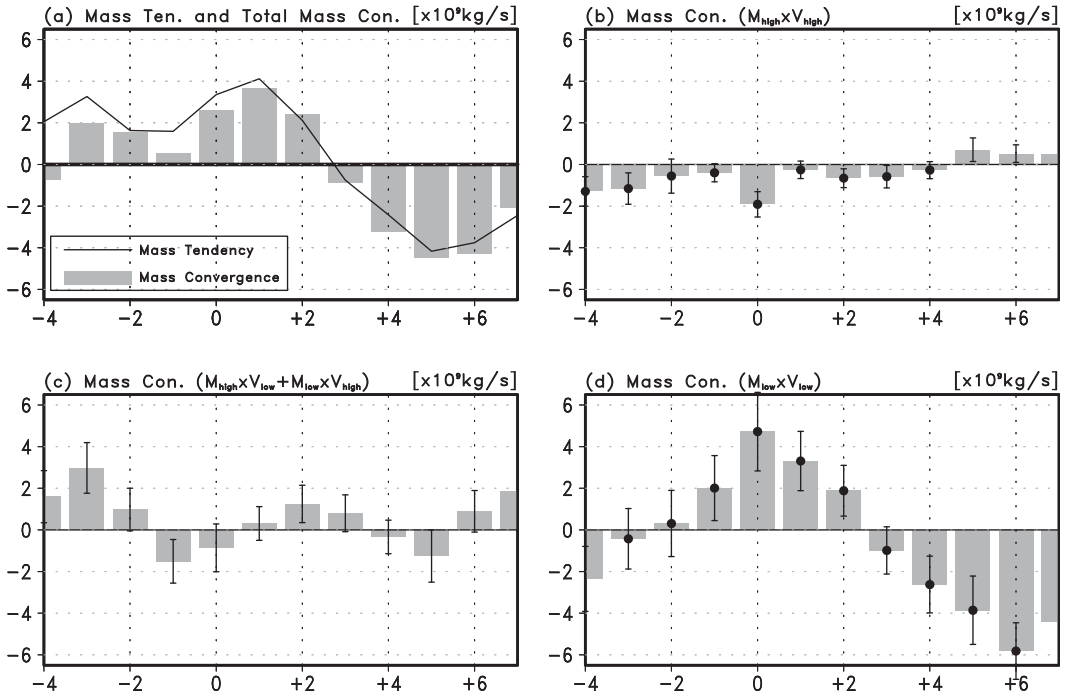

FIG. 2. (a) Temporal evolutions of the daily mass tendency (solid line) and total mass convergence evaluated from 3D mass fluxes (shaded bars) (kg s^{-1}). Mass convergence (kg s^{-1}) driven by (b) high-frequency atmospheric motions, (c) the interaction between high- and low-frequency atmospheric motions, and (d) low-frequency motions (for detailed definitions, please see section 2 of the main text). In (b)–(d), black dots indicate statistical significance at the 90% level and the error bars correspond to ±1 standard deviation error.

is clearly identified. The decay of the block is characterized by a rather rapid dissipation of mass out of the domain. Approximately 3 days after the peak intensity of the blocking, the total mass in the domain goes back to the preblocking level.

The accumulation and dissipation of the air mass over the blocking domain is further illustrated by the day-to-day mass tendency shown in Fig. 2a (solid line). Positive mass tendency lasts throughout the period from day −4 to day +2, being responsible for the eventual mass buildup while large amplitude, negative tendency dominates since day +3, indicating a rapid evacuation of mass out of the domain. Shaded bars in Fig. 2a are the mass tendencies estimated through the total mass convergence (into the blocking domain) computed on isentropic surfaces with isentropic wind and pressure data. The daily mass convergence matches the daily mass tendency (derived from pressure change) very well throughout the life cycle of the blocking event. Following Eq. (7), we decompose the total daily mass convergence into components associated with high-frequency atmospheric eddies (Fig. 2b), low-frequency eddies (Fig. 2d), and the interaction between high- and low-frequency eddies (Fig. 2c). It is quite evident that the mass convergence driven by low-frequency eddies (Fig. 2d) dictates the mass tendency during both the development and decay stage of the blocking event. High-frequency, synoptic-scale eddies (Fig. 2b), on one hand, tend to work against the low-frequency eddies by producing weak yet statistically significant mass depletion during the development stage of the blocking (from day −4 to day +2). On the other hand, mass depletion driven by high-frequency eddies during the period from day +3 to day +4 contributes positively to the decay of the blocking. That is, the transient eddy forcing plays an important role on the only depletion of mass convergence during the blocking onset, sustainment, and decay. This is in disagreement with earlier studies that demonstrated the important buildup by high-frequency disturbances in the early development of atmospheric blocks. The magnitude of the mass convergence associated with the interaction between high- and low-frequency eddies (Fig. 2c) is small compared to that associated with low-frequency eddies. Thus, Fig. 2 proves that the mass footprints of the North Pacific blocking event (i.e., the buildup and decay of the surface high) is mainly driven by atmospheric motions with a period longer than a week.

We further evaluate the vertical structure of the mass convergence during the life cycle of a blocking event.

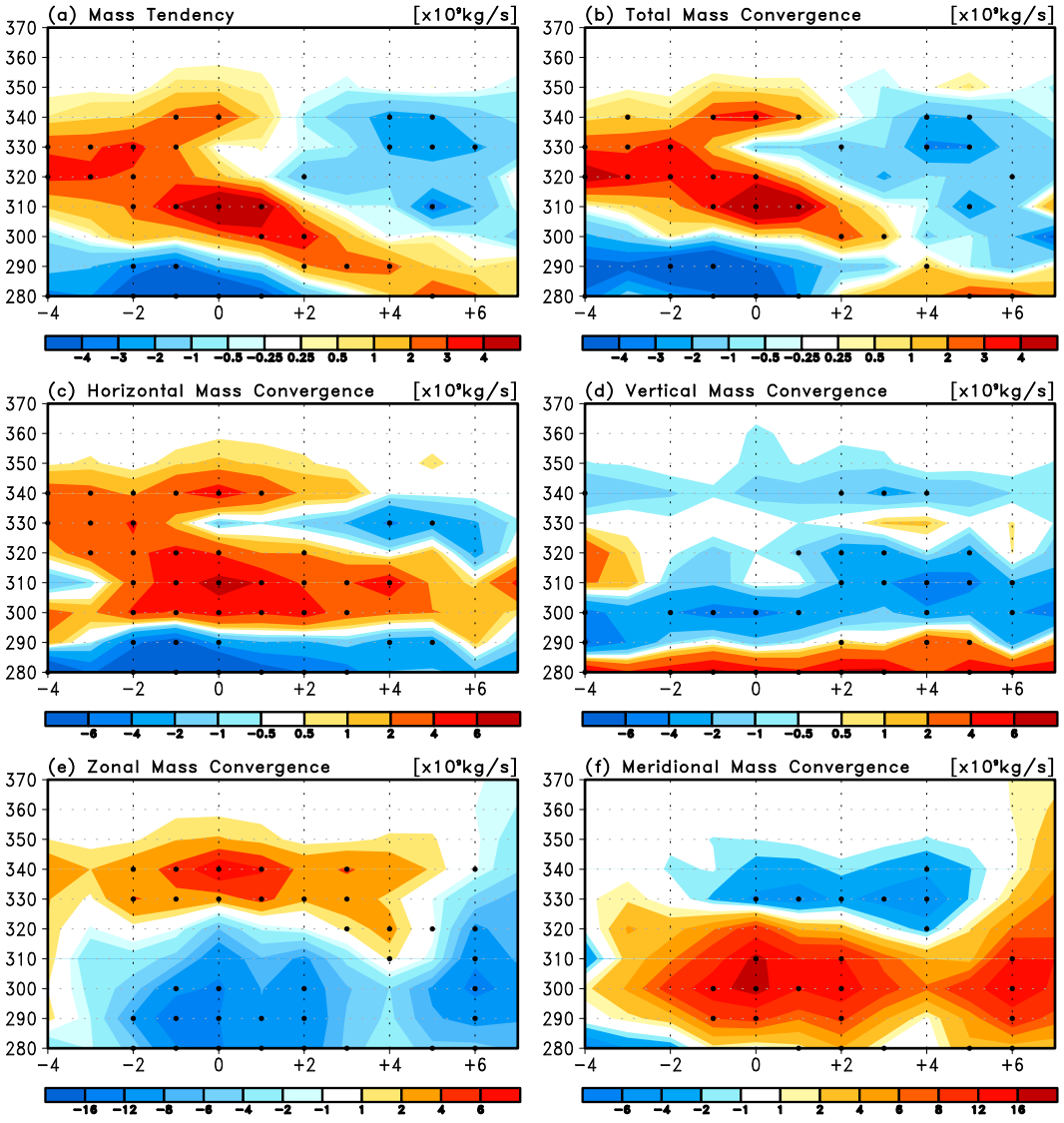

FIG. 3. Temporal evolutions of (a) the mass tendency (kg s^{-1}), and the mass convergence (kg s^{-1}) associated with (b) total, (c) horizontal, (d) vertical, (e) zonal, and (f) meridional transports for individual isentropic layers ranging from 280 to 370 K. Black dots indicate statistical significance at the 90% level.

Figure 3a plots the mass tendency derived from the isentropic level pressure change computed for individual isentropic layers between 280 and 370 K from day −4 to day +7. It agrees very well with the mass convergence shown in Fig. 3b. Prior to day +2, the mass accumulation over the blocking domain is largely caused by mass buildup between 300 and 340 K in the middle-to-upper troposphere. This buildup of mass is accompanied by relatively weak mass loss underneath 300 K. During the decay stage of the blocking (after day +2), the mass loss in the column also occurs primarily in the middle-to-upper troposphere especially in the upper troposphere between 330 and 340 K, while relatively weak mass buildup is found underneath 290 K. It is interesting to note that throughout the life cycle of the event the zone of the mass convergence propagate downward with time. The vertical structure of mass convergence is further divided into two parts: one driven by horizontal motions (Fig. 3c) and the other by vertical motions (Fig. 3d). By definition, the sum of the mass convergence associated with vertical motions in the vertical direction equals the weak vertical mass flux at 280 K, the lower boundary considered in the analysis. This is clearly the case given the significant cancellations between mass divergence (−) and convergence (+) in the vertical direction seen in Fig. 3d. As seen in Fig. 3c, horizontal

mass flux generally leads to convergence above 290 K and divergence below 290 K. This vertical dipole structure is largely compensated by the mass convergence/divergence associated with vertical transport shown in Fig. 3d. The vertical structure of the vertical mass convergence also indicates significant descent of mass from the middle-to-upper troposphere to lower troposphere during the life cycle of the blocking event.

Mass convergence associated with horizontal motions (Fig. 3c) effectively drives the total mass change over the blocking domain and its structure thus bears a high degree of similarity with that of the total mass tendency (Fig. 3a). A further separation of the horizontal mass convergence into the components related to zonal (Fig. 3e) and meridional (Fig. 3f) transports reveals the complicated roles played by zonal and meridional transports at different times in determining the overall mass footprints of an atmospheric block. The mass accumulation prior to day +2 clearly results from zonal mass convergence in the upper troposphere (320–350 K) (Fig. 3e) and meridional mass convergence in the middle-to-lower troposphere (below 320 K) (Fig. 3f). The meridional mass convergence turns out to be the dominant process given its larger vertical extent and greater value of the local maxima (~3 times of the corresponding maxima in the zonal convergence). The zonal mass convergence in the upper troposphere indicates greater zonal wind speed along the western boundary of the blocking domain compared to that along the eastern boundary, and this could be related to the westerly jet splitting that occurs during blocking. The mass dissipation after day +2, on the other hand, is mainly contributed by zonal mass divergence in the lower troposphere (below 310 K, Fig. 3e) with weak contributions from meridional divergence in the upper troposphere (around 330 K, Fig. 3f).

Figure 4 shows the breakdown of the Fig. 3 results into components associated with high-frequency and low-frequency eddies. Consistent with the previous discussion, low-frequency motions prove to be the main driver of the mass footprints of the blocking event (cf. Figs. 4b and 3b). In Fig. 4a, high-frequency eddies induce weak divergence in the upper troposphere that contributes negatively to the development of the blocking and this negative contribution overshadows even weaker positive contributions (i.e., mass convergence) in the lower troposphere. The distinct roles of the low-frequency and high-frequency eddies are also evident in terms of the mass convergence associated with horizontal motions (Figs. 4c,d). Low-frequency eddies clearly determine the overall structures of mass convergence driven by both zonal (Fig. 4f versus Fig. 3e) and meridional transport (Fig. 4h versus Fig. 3f). Note that the high- and low-frequency interaction terms are omitted here because of the lack of statistical significance.

4. Conclusions

The mass footprints associated with atmospheric blocks over the North Pacific are investigated based on the evaluation of the 3D mass fluxes and the resulted mass convergence into the blocking domain. The results highlight the critical role of mass convergence driven by low-frequency atmospheric eddies in the development and decay of a blocking event. Specifically, it is shown that low-frequency disturbances are responsible for the accelerated mass buildup a few days prior to the peak intensity of a block and they also account for the rapid mass loss during the decay stage of the block. High-frequency eddies weakly dissipate mass out of the blocking domain during most part of the blocking life cycle. It is also found that majority of the mass convergence (divergence) responsible for the intensification (decay) of the blocking high occurs in the middle-to-lower troposphere and is largely attributed to meridional (zonal) mass transport, that is, mass flux related to meridional (zonal) winds. In summary, low-frequency atmospheric eddies largely determine the mass footprints of the North Pacific atmospheric blocks with their middle-to-lower-tropospheric meridional flow dictating mass convergence for the blocking intensification and middle-to-lower-tropospheric zonal flow dictating mass divergence for the blocking decay. High-frequency eddies play an auxiliary role of dissipating mass out of the blocking zone throughout the main part of the blocking life cycle.

The present analysis is among the earliest to approach the blocking mechanism from a mass circulation perspective. It offers a different way to understand the life cycle characteristics of atmospheric blocks by quantifying processes leading to mass accumulation and dissipation during the development and decay stage of a block, respectively. One of the surprising conclusions drawn from our analysis is that the high-frequency, synoptic-scale eddies have weak negative contributions to the intensification of the blocking and weak positive contributions to the decay of the blocking. This seems to be in disagreement with earlier studies that found high-frequency eddies important for the initial development of atmospheric blocks. This difference could arise from the following: 1) earlier studies that demonstrate the importance of high-frequency eddies utilize mostly height/vorticity/potential vorticity tendency analysis that emphasizes eddy effects at specific upper-tropospheric levels (e.g., 250 hPa), while the mass flux convergence evaluated here considers a vertical integration of mass-carrying motions across multiple atmospheric levels; 2) given

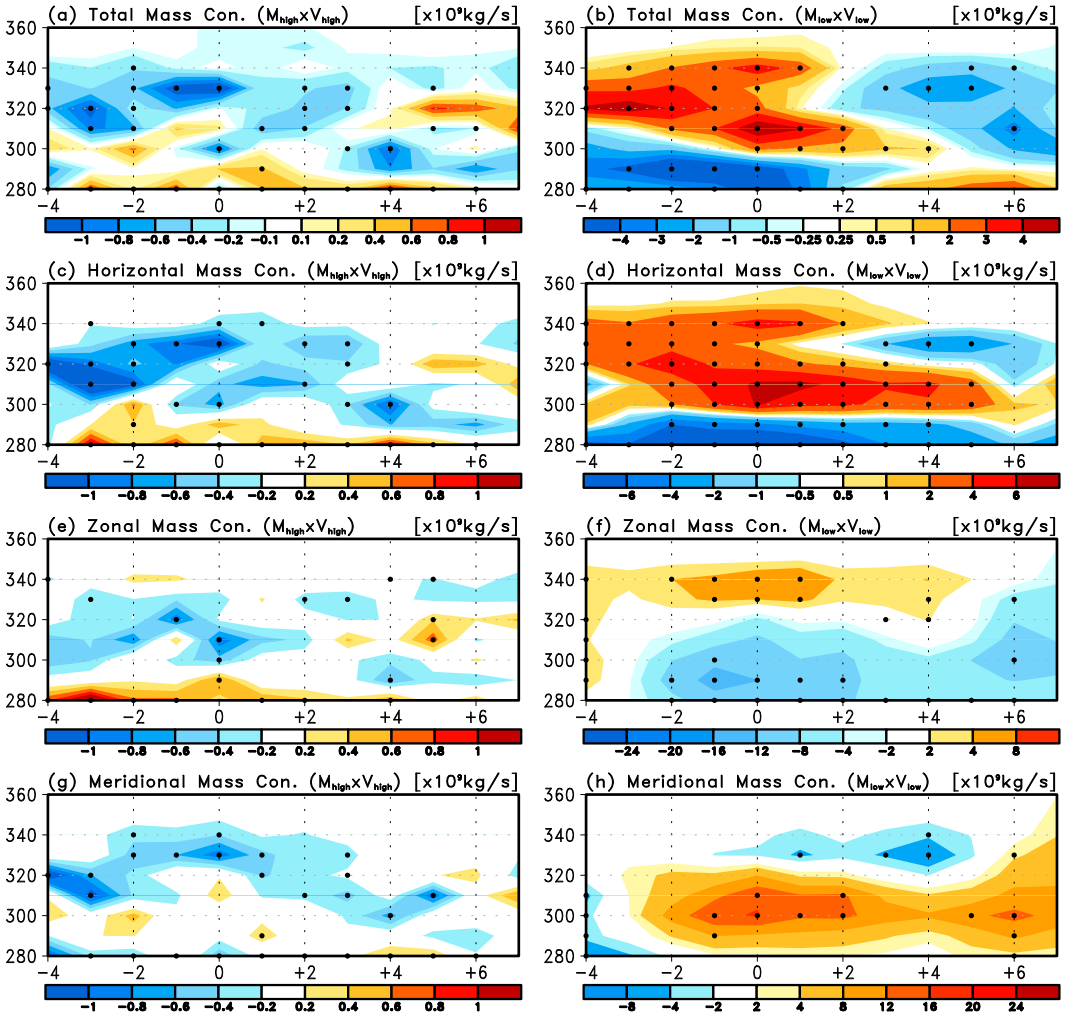

FIG. 4. Temporal evolutions of the mass convergence (kg s^{-1}) associated with (a),(b) total; (c),(d), horizontal; (e),(f) zonal; and (g),(h) meridional transports for individual isentropic layers ranging from 280 to 370 K for (left) mass convergence driven by high-frequency motions and (right) mass convergence driven by low-frequency motions. Black dots indicate statistical significance at the 90% level.

the constraint on the size of the domain, especially its zonal extent, our analysis could underestimate the role of high-frequency eddies in blocking formation especially before a well-defined positive geopotential anomaly and/or surface high becomes visible since it is known that high-frequency eddy forcing for blocking onset is typically found well upstream of the blocking area (Colucci and Alberta 1996; Mullen 1986); and 3) the high-frequency eddy forcing is probably more evident in quantities such as heat/momentum fluxes and low-frequency eddies that tend to dominate the mass-carrying motions because of their larger magnitudes. The difference of the attribution results between classic vorticity budget analysis and the mass budget analysis done here also suggests the need to further understand the cross-frequency interactions happening during blocking formation. In other words, our results do not preclude the possibility that high-frequency eddy forcing is critical in triggering blocking onset. Instead, it raised new questions such as how high-frequency eddy forcing might drive low-frequency motions that eventually lead to the mass accumulation over the blocking domain.

The new mass perspective discussed here provides a different angle to detect and trace potential model biases in simulating atmospheric blocks. Additionally, the calculations of 3D mass flux can facilitate the diagnosis of transport properties of blocking events and can be readily extended to the analysis of other classes of weather phenomena such as extratropical cyclones and hurricanes. A notable limitation of the current approach is the use of a fixed-size blocking domain since, in reality,

flow deformation (e.g., zonal stretching and meridional compression) tends to occur during the decay stage of a blocking event (Carrera et al. 2004; Croci-Maspoli et al. 2007). Further improvement of the diagnostic approach will be explored when we continue the investigation of atmospheric blocks over other geographical domains such as the Euro–Atlantic sector. It is anticipated that substantial differences in the mass footprints exist between the North Pacific and Euro–Atlantic blocks because of known differences in their dynamics (Tibaldi et al. 1997; Vial and Osborn 2012). The results of these comparisons will be reported in later publications.

Acknowledgments. We thank two anonymous reviewers whose comments and suggestions have led to a major improvement of the manuscript. The ERA-Interim data used in this study were provided by the European Centre for Medium-Range Weather Forecast (ECMWF). This study is supported by the National Science Foundation through Grants AGS-1147601 and AGS-1354402. Tae-Won Park is supported by the Korea Meteorological Administration Research and Development Program under Grant KMIPA2015-2091.

REFERENCES

Berggren, R., B. Bolin, and C. G. Rossby, 1949: An aerological study of zonal motion, its perturbations and break-down. *Tellus,* **1A,** 14–37, doi:10.1111/j.2153-3490.1949.tb01257.x.

Carrera, M. L., R. W. Higgins, and V. E. Kousky, 2004: Downstream weather impacts associated with atmospheric blocking over the northeast Pacific. *J. Climate,* **17,** 4823–4839, doi:10.1175/JCLI-3237.1.

Colucci, S. J., 1985: Explosive cyclogenesis and large-scale circulation changes—Implications for atmospheric blocking. *J. Atmos. Sci.,* **42,** 2701–2717, doi:10.1175/1520-0469(1985)042<2701:ECALSC>2.0.CO;2.

——, and T. L. Alberta, 1996: Planetary-scale climatology of explosive cyclogenesis and blocking. *Mon. Wea. Rev.,* **124,** 2509–2520, doi:10.1175/1520-0493(1996)124<2509:PSCOEC>2.0.CO;2.

Croci-Maspoli, M., C. Schwierz, and H. C. Davies, 2007: Atmospheric blocking: Space-time links to the NAO and PNA. *Climate Dyn.,* **29,** 713–725, doi:10.1007/s00382-007-0259-4.

Crum, F. X., and D. E. Stevens, 1988: A case study of atmospheric blocking using isentropic analysis. *Mon. Wea. Rev.,* **116,** 223–241, doi:10.1175/1520-0493(1988)116<0223:ACSOAB>2.0.CO;2.

Dee, D. P., and Coauthors, 2011: The ERA-Interim reanalysis: Configuration and performance of the data assimilation system. *Quart. J. Roy. Meteor. Soc.,* **137,** 553–597, doi:10.1002/qj.828.

Green, J. S. A., 1977: The weather during July 1976: Some dynamical considerations of the drought. *Weather,* **32,** 120–126, doi:10.1002/j.1477-8696.1977.tb04532.x.

Homeyer, C. R., and K. P. Bowman, 2013: Rossby wave breaking and transport between the tropics and extratropics above the subtropical jet. *J. Atmos. Sci.,* **70,** 607–626, doi:10.1175/JAS-D-12-0198.1.

Maeda, S., C. Kobayashi, K. Takano, and T. Tsuyuki, 2000: Relationship between singular modes of blocking flow and high-frequency eddies. *J. Meteor. Soc. Japan,* **78,** 631–646.

Masato, G., B. J. Hoskins, and T. J. Woollings, 2012: Wave-breaking characteristics of midlatitude blocking. *Quart. J. Roy. Meteor. Soc.,* **138,** 1285–1296, doi:10.1002/qj.990.

Moore, J. T., 1989: Isentropic analysis and interpretation: Operational applications to synoptioc and mesoscale forecast problems. Defense Technical Information Center, 93 pp.

Mullen, S. L., 1986: The local balances of vorticity and heat for blocking anticyclones in a spectral general circulation model. *J. Atmos. Sci.,* **43,** 1406–1441, doi:10.1175/1520-0469(1986)043<1406:TLBOVA>2.0.CO;2.

Nakamura, H., and J. M. Wallace, 1993: Synoptic behavior of baroclinic eddies during the blocking onset. *Mon. Wea. Rev.,* **121,** 1892–1903, doi:10.1175/1520-0493(1993)121<1892:SBOBED>2.0.CO;2.

——, M. Nakamura, and J. L. Anderson, 1997: The role of high- and low-frequency dynamics in blocking formation. *Mon. Wea. Rev.,* **125,** 2074–2093, doi:10.1175/1520-0493(1997)125<2074:TROHAL>2.0.CO;2.

Pelly, J. L., and B. J. Hoskins, 2003: A new perspective on blocking. *J. Atmos. Sci.,* **60,** 743–755, doi:10.1175/1520-0469(2003)060<0743:ANPOB>2.0.CO;2.

Rex, D. F., 1950: Blocking action in the middle troposphere and its effect upon regional climate. *Tellus,* **2A,** 196–211, doi:10.1111/j.2153-3490.1950.tb00331.x.

Shutts, G. J., 1983: The propagation of eddies in diffluent jetstreams: Eddy vorticity forcing of 'blocking' flow fields. *Quart. J. Roy. Meteor. Soc.,* **109,** 737–761, doi:10.1002/qj.49710946204.

Stewart, D. A., 1993: Persistent anomaly forcing in a two-level global circulation model. *J. Atmos. Sci.,* **50,** 2710–2730, doi:10.1175/1520-0469(1993)050<2710:PAFIAT>2.0.CO;2.

Tibaldi, S., F. D'Andrea, E. Tosi, and E. Roeckner, 1997: Climatology of Northern Hemisphere blocking in the ECHAM model. *Climate Dyn.,* **13,** 649–666, doi:10.1007/s003820050188.

Trigo, R. M., I. F. Trigo, C. C. DaCamara, and T. J. Osborn, 2004: Climate impact of the European winter blocking episodes from the NCEP/NCAR Reanalyses. *Climate Dyn.,* **23,** 17–28, doi:10.1007/s00382-004-0410-4.

Vial, J., and T. Osborn, 2012: Assessment of atmosphere-ocean general circulation model simulations of winter northern hemisphere atmospheric blocking. *Climate Dyn.,* **39,** 95–112, doi:10.1007/s00382-011-1177-z.

Ziv, B., and P. Alpert, 1994: Isobaric to isentropic interpolation errors and implication to potential vorticity analysis. *J. Appl. Meteor.,* **33,** 694–703, doi:10.1175/1520-0450(1994)033<0694:ITIIEA>2.0.CO;2.